Evidence for *s*-wave pairing from measurement of the lower critical field in $MgCNi_3$

X. F. Lu, L. Shan, Z. Wang, H. Gao, Z. A. Ren, G. C. Che, and H. H. Wen*
National Laboratory for Superconductivity, Institute of Physics, Chinese Academy of Sciences, P.O. Box 603, Beijing 100080, People's Republic of China
(Received 23 May 2004; revised manuscript received 7 September 2004; published 27 May 2005)

Magnetization measurements in the low-field region have been carefully performed on a well-shaped cylindrical and an ellipsoidal sample of superconductor $MgCNi_3$. Data from both samples show almost the same results. The lower critical field H_{c1} and the London penetration depth λ are thus derived. It is found that the result of normalized superfluid density $\lambda^2(0)/\lambda^2(T)$ of $MgCNi_3$ can be well described by BCS prediction with the expectation for an isotropic *s*-wave superconductivity.

DOI: 10.1103/PhysRevB.71.174511 PACS number(s): 74.25.Bt, 74.25.Ha, 74.70.Dd

I. INTRODUCTION

The pairing symmetry is very essential for uncovering the mechanism both for conventional and high-T_c superconductivity. The recently discovered intermetallic perovskite $MgCNi_3$ superconductor[1] is regarded as a bridge between conventional superconductors and high-T_c cuprates, and the issue concerning its symmetry of order parameter has attracted considerable attention. However, pairing symmetry about $MgCNi_3$ remains highly controversial in the literature. NMR,[2] specific heat,[3] scanning tunneling measurements,[4] point contact tunneling spectra[5] and density functional calculations[6,7] favor the *s*-wave pairing in $MgCNi_3$. On the other hand, the theoretical calculation,[8] some tunneling spectra[9] and the penetration depth measurement[10] support non-*s*-wave superconductivity. Recently a two-band *s*-wave model has been proposed by Wälte *et al.*[11] who try to explain the complex behavior observed in $MgCNi_3$.

In this paper, we derive the thermodynamic parameters H_{c1} and λ of two $MgCNi_3$ samples by careful magnetization measurement. It is found that the normalized superfluid density $\lambda^2(0)/\lambda^2(T)$ can be described by BCS prediction for a *s*-wave pairing symmetry. Therefore, our magnetization data support the conventional single band *s*-wave superconductivity in $MgCNi_3$.

This paper is organized as follows. The samples and experimental details are presented in Sec. II. The data and discussions are given in Sec. III. Section IV gives the summary.

II. SAMPLES AND EXPERIMENTAL DETAILS

The polycrystalline $MgCNi_3$ sample investigated here has been prepared by powder metallurgy method, and the details of preparation can be found elsewhere.[12] The superconducting transition temperature is 6.9 K measured by both magnetization [ac susceptibility (f=333 Hz, H_{ac}=1 Oe) and dc diamagnetization shown in Fig. 1(a)] and resistivity measurement. The $M(T)$ curves show a sharp transition with the transition width less than 0.5 K. The x-ray diffraction (XRD) analysis presented in Fig. 1(b) shows that all diffraction peaks are from the $MgCNi_3$ phase, which indicates that the sample is nearly of single phase.

In order to minimize the demagnetization factor, one sample (denoted as *S*-*c*) has been carefully cut and ground to a cylinder with a diameter of 1.1 mm and length of 7.0 mm. The demagnetization factor in this situation is almost negligible since the field has been applied along the axis of the cylinder. Another sample (denoted as *S*-*e*) has been polished to an ellipsoid with semimajor axis a=3.74 mm and semiminor axis b=1.5 mm. The demagnetization factor for the ellipsoidal sample is $n=(1-1/e^2)\{1-1/2e\ \ln[(1+e)/(1-e)]\} \approx 0.136$, with $e=\sqrt{1-b^2/a^2}$. The magnetic fields have been applied parallel to the longitudinal axis of the samples.

The magnetic measurements are mainly carried out on an Oxford cryogenic MagLab system (MagLab12Exa, with temperature down to 1.5 K) and checked by a quantum design superconducting interference device (SQUID, MPMS 5.5 T). After zero-field cooled (ZFC) from 25 K to a desired temperature, the magnetization curve $M(H)$ is measured with the applied magnetic field swept slowly up to 1000 Oe

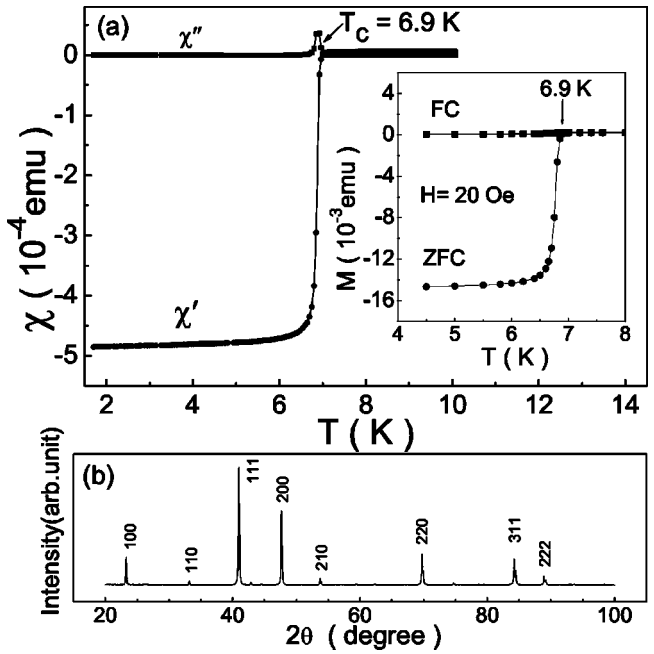

FIG. 1. (a) The ac susceptibility curves of $MgCNi_3$ measured by MagLab with ac field 1 Oe and frequency 333 Hz. The inset gives the ZFC and FC dc diamagnetization at 20 Oe measured by SQUID. (b) XRD patterns of the $MgCNi_3$.

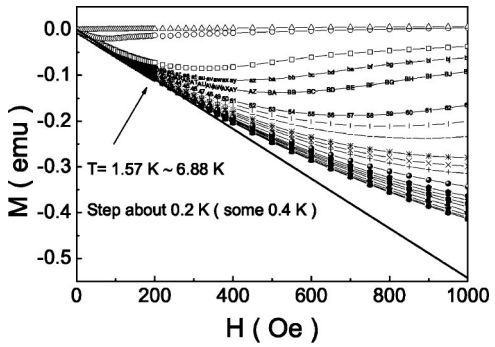

FIG. 2. The magnetization curves of $M(H)$ for $MgCNi_3$. The solid line is the "Meissner line" defined in the text. The temperature is varied from 1.57 to 6.88 K from bottom to top, with step about 0.2 K (some 0.4 K). It is found that the initial slope of all the curves is the same.

($\gg H_{c1}$). It is important to note that the magnet has been degaussed at $T=25$ K in order to eliminate the remanent field before each measurement. It is essential to do degaussing since otherwise even 5 Oe residual field may cause significant effect on the result of magnetization.

III. EXPERIMENTAL DATA AND DISCUSSIONS

In this section, the processes to obtain the superconducting parameters by magnetization measurement have been reported in detail for two $MgCNi_3$ samples, one is a cylinder and another is an ellipsoid.

A. The cylindrical sample (*S*-*c*)

The curves of dc magnetization are shown in Fig. 2. The temperature varies between 1.57 and 6.88 K with steps 0.2 K (some 0.4 K). All curves clearly show the common linear dependence of the magnetization on field caused by Meissner effect at low fields, and this extrapolated common line is the so-called "Meissner line" (ML). The optimal ML (solid line in Fig. 2) is achieved by doing linear fit $M(H)$ of the lowest temperature (1.57 K) at low fields, which represents the magnetization curve of Meissner state. The value of H_{c1} is determined by examining the point of departure from linearity on the initial slope of the magnetization curve (ML) with a certain criterion. The results of subtracting this ML from magnetization curves are plotted in Fig. 3 and the ΔM between 7.0×10^{-4} and 1.4×10^{-3} emu are shown in the inset with an enlarged view. All curves show a fast drop to the resolution of device when the real H_{c1} is approached, so the value of H_{c1} is easily obtained by choosing a proper criterion of ΔM. The $H_{c1}(T)$ acquired by using criteria of $\Delta M=7.0\times10^{-4}$ and 1.1×10^{-3} emu are shown in Fig. 4. Then the penetration depth $\lambda(T)$ can be achieved from $H_{c1}(T)$ by

$$H_{c1}=\frac{\Phi_0}{4\pi\lambda^2}\ln\kappa \tag{1}$$

and they are displayed in the inset of Fig. 4. Here $\Phi_0=hc/2e\approx2\times10^{-7}$ G cm^2 is the flux quantum and κ is the

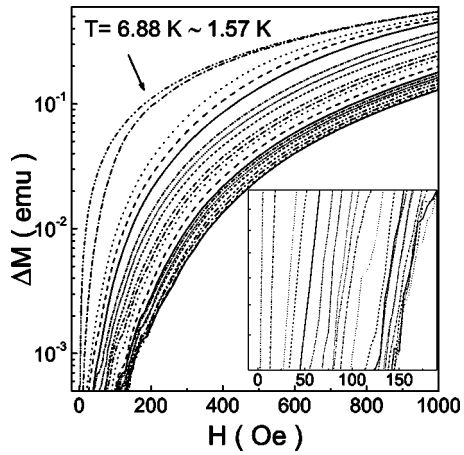

FIG. 3. The difference between the "Meissner line" and the $M(H)$ curves. ΔM is shown in logarithmic scale. The inset shows the enlarged ΔM (between 7.0×10^{-4} and 1.4×10^{-3} emu).

Ginzburg-Landau parameter. We take κ as constant since it is a weakly temperature-dependent parameter.

The values of nominal H_{c1} and λ seem to be criterion dependent in this method, however, temperature dependence of H_{c1} and $\lambda(T)$ are found to be weakly criterion dependent if the data are normalized by the zero temperature values [see $\lambda^2(0)/\lambda^2(T)$ in Fig. 5]. In addition, ΔM drops sharply with decreasing magnetic field, the use of lower ΔM value in our criterion will not result in a much different $H_{c1}(T)$ curve. If not specially mentioned, the discussion is based on the data using the criterion of 7.0×10^{-4} emu hereinafter. At the temperatures below 2.8 K ($<0.4\ T_c$), the values of $H_{c1}(T)$ and $\lambda(T)$ are almost constant despite the lack of the data below 1.5 K. This may imply the conventional *s*-wave nature in $MgCNi_3$, because the finite energy gap manifests itself with an exponentially activated temperature dependence of thermodynamic parameters. This can be further confirmed in the following discussion on superfluid density. It is worth noting that it is very difficult to distinguish a slight difference of H_{c1} (or $1/\lambda^2$) in the low-temperature region between different pairing symmetries, for example, for an ideal *s*-wave, an exponential dependence is anticipated, for a dirty *d* wave, a quadratic form $\rho_s(T)=\rho_s(0)-\alpha T^2$ is expected. Here we use

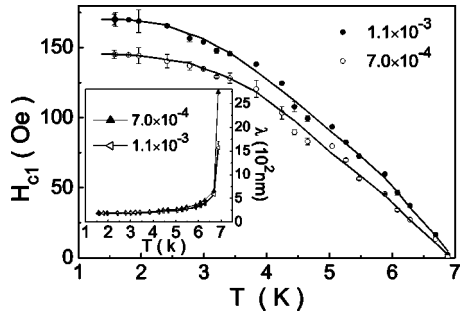

FIG. 4. The temperature dependence of the nominal H_{c1} and λ (inset). $H_{c1}(T)$ is obtained by using criterion of $\Delta M=7.0\times10^{-4}$ (open circles) and 1.1×10^{-3} emu (solid circles), respectively. Error bars are given for determining the nominal H_{c1} and λ. Lines are guides to the eyes.

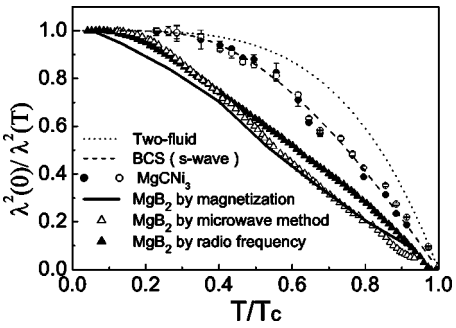

FIG. 5. The temperature dependence of $\lambda^2(0)/\lambda^2(T)$ for $MgCNi_3$ and MgB_2. The values of $\lambda^2(0)/\lambda^2(T)$ are obtained by $H_{c1}(T)$ using criteria of ΔM equal to 7.0×10^{-4} (open circles) and 1.1×10^{-3} emu (solid circles) for $MgCNi_3$ and 1.0×10^{-4} emu for MgB_2 (solid). The prediction by two-fluid model (dotted) and BCS *s*-wave (dashed) are also shown. The data of open and solid triangles are the experimental measurement by microwave resonator method and radio frequency technique for MgB_2, respectively (from Refs. 18 and 19).

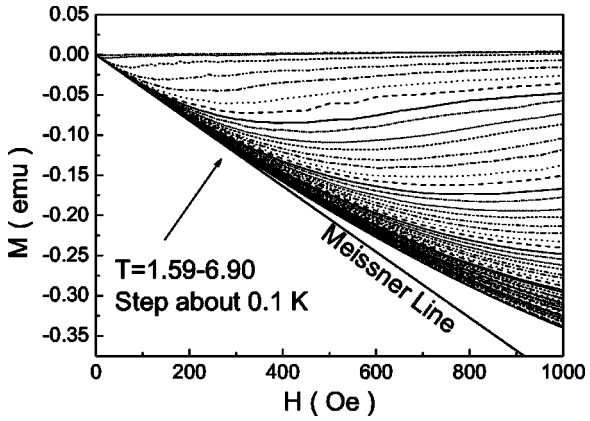

FIG. 6. The magnetization curves of $M(H)$ for the ellipsoidal $MgCNi_3$ sample. The solid line is the "Meissner line." The temperature is varied from 1.59 to 6.90 K (from bottom to top), with steps of about 0.1 K.

an alternative way, i.e., to fit the data in intermediate and high-temperature region to extract useful message for pairing symmetry.

As we know, the total superfluid density ρ_s is proportional to $\lambda^{-2}(T)$, and $\lambda^2(0)/\lambda^2(T)$ represents the normalized superfluid density. In Fig. 5, we display the temperature dependence of $\lambda^2(0)/\lambda^2(T)$ of $MgCNi_3$ with $\lambda(0)$ as a fit parameter. The predictions of BCS *s*-wave (dashed) and two-fluid model (dotted) are also shown. According to the BCS theory for clean superconductors,[13,14] the normalized superfluid density $\lambda^2(0)/\lambda^2(T)$ is expressed as follows:

$$\frac{\lambda^2(0)}{\lambda^2(T)} = 1 - 2\int_{\Delta(T)}^{\infty}\left(-\frac{\partial f(E)}{\partial E}\right)D(E)dE, \tag{2}$$

where $\Delta(T)$ is the BCS superconducting energy gap, $f(E) = 1/[\exp(-E/k_BT)+1]$ is the Fermi distribution function, and $D(E)=E/[E^2-\Delta^2(T)]^{1/2}$ is the quasiparticle density of states. The most appropriate superconducting gap $\Delta(0)=1.86k_BT_c$ is chosen in our BCS calculation with $T_c=6.9$ K, and this value is reasonable for $MgCNi_3$ because the generally reported results are larger than the conventional BCS value $(1.76k_BT_c)$. It is found that $\lambda^2(0)/\lambda^2(T)$ of $MgCNi_3$ can be well described by the *s*-wave BCS theory with a single gap, but the two-fluid model shows a substantial deviation. This suggests the *s*-wave nature of superconductivity in $MgCNi_3$, which is consistent with our previous conclusion reached by point-contact tunneling.[5] Later on we will show that our results are not compatible with any other pairing symmetry with nodes on the gap function which normally contributes a power law dependence to the temperature dependence ρ_s.

For the sake of comparison, the temperature dependence of the normalized superfluid density in MgB_2 obtained by exactly the same magnetization method[15] is also shown in Fig. 5, with $\lambda(0)$ as a fit parameter. Clearly the data cannot be understood in isotropic *s*-wave BCS theory or two-fluid model because of the two-gap characteristic of MgB_2.[16,17] The data obtained from this simple magnetization method on MgB_2 were found to be close to that determined by more elegant microwave method[18] and radio frequency technique,[19] which can be seen from Fig. 5. This indicates that the same magnetization method used in $MgCNi_3$ to get H_{c1} and λ is reliable, and the corresponding results are plausible.

One may argue whether the H_{c1} obtained here is the lower critical field of grains because of the polycrystalline nature of our sample. In our magnetization experiment, the nominal $H_{c1}(0)$ of our sample is about 145.1 Oe. Combined with $H_{c2}(0)$ $(1.18\times10^5$ Oe) determined from our previous measurement of specific heat,[20] we can reach that the value of κ is 39 and $H_c(0)$ equals to 2165 Oe by Eqs. (3) and (4). The value of coherence length is 5.3 nm obtained by Eq. (5).

$$H_{c1}(T) = \frac{1}{\sqrt{2}}H_c(T)\frac{1}{\kappa}\ln\kappa, \tag{3}$$

$$H_{c2}(T) = \sqrt{2}H_c(T)\kappa, \tag{4}$$

$$\xi(0) = \sqrt{\Phi_0/2\pi H_{c2}(0)}. \tag{5}$$

The value of $\lambda(0)$ is about 200.1 nm. All these values of parameters are in the range of the reported results of $MgCNi_3$ by other techniques (see collected parameters in Ref. 11). This manifests that H_{c1} measured here reflects the bulk property. In addition, the value of ξ for $MgCNi_3$ is quite large, so that the influence of the grain boundary is weak.

Another argument is that the nominal H_{c1} relation obtained in our experiment may not reflect the true H_{c1} but the flux entry field because of the Bean-Livingston surface barrier and effects of sample corners geometrical barriers. However, we would argue that the influence of surface barrier is not important to our cylindrical sample, since the magnetization hysteresis loops are very symmetric in the temperature and field regimes we measured. In order to further verify the validity of this method to obtain H_{c1}, we have repeated the same measurement for an ellipsoidal sample. The data and the discussion are presented below.

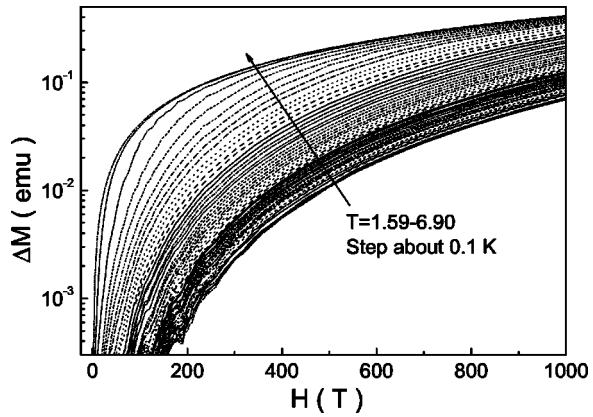

FIG. 7. The difference between the "Meissner line" and the $M(H)$ curves. ΔM is shown in logarithmic scale.

B. The ellipsoidal sample (*S*-*e*)

The curves of dc magnetization are shown in Fig. 6 and the temperature varies between 1.59 and 6.90 K with steps about 0.1 K. The optimal "Meissner line" (solid line in Fig. 6) has been determined in the same way as for the cylindrical sample. Subtracting this ML from the magnetization data yields the ΔM curves plotted in Fig. 7. The $H_{c1}(T)$ acquired by using criteria of $\Delta M = 3.2\times10^{-4}$ and 1.0×10^{-3} emu are shown in Fig. 8, and the demagnetization factor n ($\approx$0.136) has been taken into account. Then the penetration depth $\lambda(T)$ can be achieved from Eq. (1) and they are displayed in the inset of Fig. 8. The normalized temperature dependence of $\lambda^2(0)/\lambda^2(T)$ of $MgCNi_3$ is shown in Fig. 9. One can clearly see that the data from the ellipsoidal sample are almost identical to that for the cylindrical sample, showing a trivial influence of either the geometrical or surface barrier in our present samples.

In addition, we have calculated the superfluid density assuming a nodal gap with *d*-wave symmetry. Under the frame of the BCS theory, if the gap has a *d*-wave-like node, the normalized superfluid density $\lambda^2(0)/\lambda^2(T)$ is written as

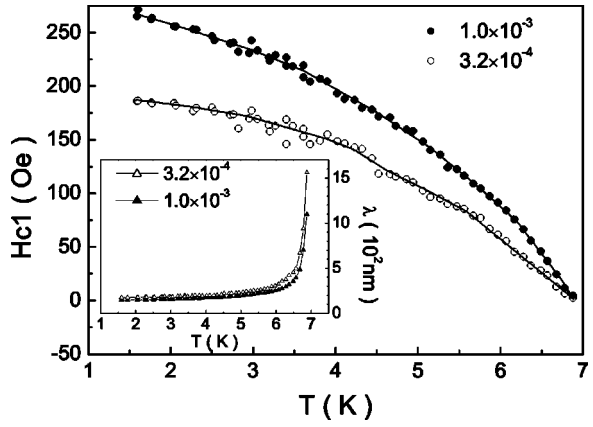

FIG. 8. The temperature dependence of the nominal H_{c1} and λ (inset). Lines are guides to the eyes.

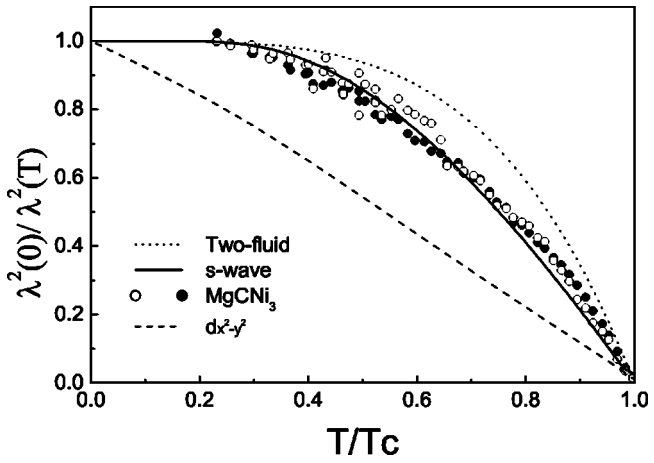

FIG. 9. The temperature dependence of $\lambda^2(0)/\lambda^2(T)$ for ellipsoidal $MgCNi_3$ sample. The values of $\lambda^2(0)/\lambda^2(T)$ are obtained by $H_{c1}(T)$ using criteria of ΔM equal to 3.2×10^{-4} (open circles) and 1.0×10^{-3} emu (solid circles). The prediction by two-fluid model (dotted), BCS *s*-wave (solid) and pure *d*-wave (dashed) are also shown.

$$\frac{\lambda^2(0)}{\lambda^2(T)} = 1 - \frac{1}{\pi}\int_0^{2\pi}\int_{\Delta(T,\theta)}^{\infty} -\frac{\partial f(E)}{\partial E} D(E)\,dE\,d\theta \qquad (6)$$

with $f(E)=1/[\exp(-E/k_BT)+1]$, $\Delta(T,\theta)=\Delta_0(T)\cos 2\theta$ and $D(E)=E/[E^2-\Delta^2(T,\theta)]^{1/2}$. The calculated *d*-wave results are shown in Fig. 9 with dashed line. For p_x-wave symmetry with $\Delta(T,\theta)=\Delta_0(T)\sin\theta$, we found that the calculated temperature dependence of $\lambda^2(0)/\lambda^2(T)$ is close to that of a *d*-wave, and far from our experiment data. The predictions of *s*-wave BCS (solid) and two-fluid model (dotted) are also shown in Fig. 9. It is found that our data can only be well described by the *s*-wave model. Together with the results for the cylindrical sample, we conclude that $MgCNi_3$ is most likely an isotropic *s*-wave superconductor.

IV. SUMMARY

To summarize, we have measured the *M*-*H* curves of two $MgCNi_3$ samples with cylindrical and ellipsoidal shapes and obtained their lower critical field $H_{c1}(T)$ and $\lambda(T)$. The temperature dependence of normalized superfluid density is consistent with the *s*-wave BCS theory. All these indicate that $MgCNi_3$ may possess an isotropic *s*-wave gap, which is in sharp contrast to MgB_2.

Note added. The recent report of carbon isotope effect in $MgCNi_3$ by T. Klimczuk and R. J. Cava indicates that carbon-based phonons play an essential role in the superconducting mechanism.[21]

ACKNOWLEDGMENTS

This work was supported by the National Science Foundation of China, the Ministry of Science and Technology of China, and the Chinese Academy of Sciences within the knowledge innovation project.

*Electronic address: hhwen@aphy.iphy.ac.cn

[1] T. He, Q. Huang, A. P. Ramirez, Y. Wang, K. A. Regan, N. Rogado, M. A. Hayward, M. K. Haas, J. S. Slusky, K. Inumara, H. W. Zandbergen, N. P. Ong, and R. J. Cava, Nature (London) **411**, 54 (2001).

[2] P. M. Singer, T. Imai, T. He, M. A. Hayward, and R. J. Cava, Phys. Rev. Lett. **87**, 257601 (2001).

[3] J. Y. Lin, P. L. Ho, H. L. Huang, P. H. Lin, Y. L. Zhang, R. C. Yu, C. Q. Jin, and H. D. Yang, Phys. Rev. B **67**, 052501 (2003).

[4] G. Kinoda, M. Nishiyama, Y. Zhao, M. Murakami, N. Koshizuka, and T. Hasegawa, Jpn. J. Appl. Phys., Part 2 **40**, L1365 (2001).

[5] L. Shan, H. J. Tao, H. Gao, Z. Z. Li, Z. A. Ren, G. C. Che, and H. H. Wen, Phys. Rev. B **68**, 144510 (2003).

[6] D. J. Singh and I. I. Mazin, Phys. Rev. B **64**, 140507 (2001).

[7] A. Yu. Ignatov, S. Y. Savrasov, and T. A. Tyson, Phys. Rev. B **68**, 220504 (2003).

[8] H. Rosner, R. Weht, M. D. Johannes, W. E. Pickett, and E. Tosatti, Phys. Rev. Lett. **88**, 027001 (2002).

[9] Z. Q. Mao, M. M. Rosario, K. D. Nelson, K. Wu, I. G. Deac, P. Schiffer, Y. Liu, T. He, K. A. Regan, and R. J. Cava, Phys. Rev. B **67**, 094502 (2003).

[10] R. Prozorov, A. Snezhko, T. He, and R. J. Cava, Phys. Rev. B **68**, 180502(R) (2003).

[11] A. Wälte, G. Fuchs, K. H. Müller, A. Handstein, K. Nenkov, V. N. Narozhnyi, S. L. Drechsler, S. Shulga, and L. Schultz, cond-mat/0402421 (unpublished).

[12] Z. A. Ren, G. C. Che, S. L. Jia, H. Chen, Y. M. Ni, G. D. Liu, and Z. X. Zhao, Physica C **371**, 1 (2002).

[13] M. Tinkham, *Introduction to Superconductivity*, 2nd ed. (McGraw-Hill, New York, 1996), p. 93.

[14] M. S. Kim, J. A. Skinta, T. R. Lemberger, W. N. Kang, H. J. Kim, E. M. Choi, and S. I. Lee, Phys. Rev. B **66**, 064511 (2002).

[15] S. L. Li, H. H. Wen, Z. W. Zhao, Y. M. Ni, Z. A. Ren, G. C. Che, H. P. Yang, Z. Y. Liu, and Z. X. Zhao, Phys. Rev. B **64**, 094522 (2001).

[16] H. J. Choi, D. Roundy, H. Sun, M. L. Cohen, and S. G. Louie, Nature (London) **418**, 758 (2001).

[17] B. Kang, H. J. Kim, M. S. Park, K. H. Kim, and S. I. Lee, cond-mat/0403140 (unpublished).

[18] N. Klein, B. B. Jin, R. Wördenweber, P. Lahl, W. N. Kang, Hyeong-Jin Kim, Eun-Mi Choi, Sung-IK Lee, T. Dahm, and K. Maki, IEEE Trans. Appl. Supercond. **13**, 3253 (2003).

[19] F. Manzano, A. Carrington, N. E. Hussey, S. Lee, A. Yamamoto, and S. Tajima, Phys. Rev. Lett. **88**, 047002 (2002).

[20] L. Shan, K. Xia, Z. Y. Liu, H. H. Wen, Z. A. Ren, G. C. Che, and Z. X. Zhao, Phys. Rev. B **68**, 024523 (2003).

[21] T. Klimczuk and R. J. Cava, cond-mat/0410504 (unpublished).